

Knudsen Diffusion Through Cylindrical Tubes of Varying Radii: Theory and Monte Carlo Simulations

Yong Shi · Yong Taek Lee · Albert S. Kim

Received: 6 April 2011 / Accepted: 15 February 2012 / Published online: 6 March 2012
© Springer Science+Business Media B.V. 2012

Abstract In this study, Knudsen diffusion of low-pressure gases of infinite mean free path through various tubes is studied using the integral equation theory (IET), standard diffusion theory, and Monte Carlo (MC) simulations. We investigated the transmission probabilities (TPs) of linearly diverging–converging, sinusoidally bulging, and periodic tubes as compared with TPs of conventional straight cylinders. An exact analytic solution for the TP through the straight cylindrical tube was developed using the standard diffusion theory with a linear concentration approximation. IET for the TPs through the diverging–converging and bulging tubes were developed. MC simulation techniques were applied to calculate TPs through all the tube types azimuthal symmetry of which was held with tube radius changing only along the axial coordinate (z). The linearly diverging–converging and sinusoidally bulging tubes provide noticeably higher TPs than those of the equivalent straight tubes. Periodic tubes show that if the tube length scaled by the equivalent diameter is of an order of or greater than the periodicity coefficient (equal to the number of peaks on the tube wall), then the TP of the periodic tube is larger than that of the equivalent straight tube.

Keywords Knudsen transport · Periodic tube · Transmission probability · Integral equation theory · Monte Carlo simulation

Y. Shi · A. S. Kim (✉)
Civil and Environmental Engineering, University of Hawaii at Manoa,
2540 Dole Street, Honolulu, HI 96822, USA
e-mail: albertsk@hawaii.edu

Y. Shi
e-mail: yongshi@hawaii.edu

Y. T. Lee · A. S. Kim
Chemical Engineering, College of Engineering, Kyung Hee University,
Gyeonggi-do 449-701, South Korea
e-mail: yongtlee@khu.ac.kr

List of Symbols

\bar{v}	Mean molecular speed
β	Angle at the inlet and outlet of the diverging–converging tube in magnitude
ε	Peak amplitude of tube, i.e., a dimensionless distance from the imaginary tube surface of radius r_0 at the mid-point (at $z = L/2$) to the peak of the diverging–converging or bulging tube
$\eta_{\text{dir}}^{\text{C}}$	Direct TP of Clausing’s analytic solution, taken from Walsh’s work
$\eta_{\text{dir}}^{\text{SKL, MC}}$	Direct TP calculated using Monte Carlo simulations in this study
$\eta_{\text{ind}}^{\text{SKL, MC}}$	Indirect TP calculated using Monte Carlo simulations in this study
$\eta_{\text{tot}}^{\text{SKL}}$	Total TP as a summation of direct TP by Clausing’s integral equation theory and indirect TP by our theory developed in this study
$\eta_{\text{dir}}^{\text{PP}}$	Direct TP of Pollard & Present’s theory for the first-order correction
$\eta_{\text{dir}}^{\text{W, Asym}}$	Direct TP of Walsh’s asymptotic form
$\eta_{\text{ind}}^{\text{C, Asym}}$	Indirect TP of Clausing’s asymptotic form
$\eta_{\text{ind}}^{\text{K}}$	Indirect TP corresponding to the original Knudsen diffusivity, D_{K}
$\eta_{\text{ind}}^{\text{PP}}$	Indirect TP of Pollard & Present’s theory for the first-order correction
$\eta_{\text{ind}}^{\text{SKL}}$	Indirect TP analytically derived in this study
$\eta_{\text{tot}}^{\text{PP}}$	Total TP of Pollard & Present’s theory for the first-order correction
λ	Mean free length of molecules
$\omega(z)$	Escape probability that the molecule at z will pass the (right) outlet without returning to the left reservoir
a	Radius of a straight cylindrical tube
d	Diameter of a straight cylindrical tube
$d_{\text{eq}}^{\text{bulging}}$	Equivalent diameter of this bulging tube
d_{eq}	Equivalent diameter of a tube of an axially varying diameter having the identical void volume and length of a straight tube
$d_{\text{eq}}^{\text{div-conv}}$	Equivalent diameter of the conically diverging–converging tube of Eq. 10
D_{K}	Knudsen diffusivity for a semi-infinitely long tube of diameter d
$d_p(z)$	Diameter of a tube as a function of the axial position z
L	Length of a tube
L'	Half length of a tube
$L_{\text{cross}}/d_{\text{eq}}$	Dimensionless crossing distance at which the TPs of periodic and straight tubes are identical
M	Molecular weight
$n(z)$	Number concentration of molecules in the tube
n_1	Number concentration of molecules at the tube inlet
n_2	Number concentration of molecules at the tube outlet
N_w	Number of molecules passing through the central cross-sectional area per unit time
$r(z)_{\text{bulging}}$	Radius of the bulging (sinusoidally diverging–converging) tube
$r(z)_{\text{div-conv}}$	Radius of the conically diverging–converging tube
r'	Distance of molecules, traveling without collisions
r_0	Inlet and outlet radius of diverging–converting and bulging tubes
$r_1(z)$	Radius at the left side of the diverging–converting/bulging tube

$r_2(z)$	Radius at the right side of the diverging–converting/bulging tube
T	Temperature
V	Volume of void spaces in a tube
z	Axial coordinate of a tube

1 Introduction

The Knudsen diffusion (KD) phenomenon of gases through narrow pores was discovered more than a century ago (Knudsen 1909; Knudsen and Fisher 1910), but it still remains as a partially unsolved problem due to chemical, physical, and more importantly geometrical complexities of porous media. For a low-pressure gas passing through a long tube, the mean free path of the gas molecules (as a function of temperature in general) can be much larger than the pore dimensions. The majority of traveling gas molecules collide with the internal tube wall. Inter-molecular collisions rarely occur in this low concentration system, and therefore the normal Brownian diffusion does not play a significant role in the diffusive gas transport. If a constant pressure gradient exists along the tube by maintaining fixed concentrations at the inlet and outlet, then KD is the dominant transport mechanism of the low-pressure gas and can be effectively used for separation of binary or mixed gases in various engineering applications such as isotope separation (Villani 1976), hydrogen extraction (Kogan 1998), and membrane distillation (MD) (Calabro et al. 1994; Diban et al. 2009). A comprehensive review of MD can be found elsewhere (Curcio and Drioli 2005).

The KD coefficient, i.e., the proportionality between diffusive gas flux and the concentration gradient, has the asymptotic form of $D_K = \frac{1}{3}\bar{v}d$ for a long tube of length $L (\gg d)$, where \bar{v} is the mean molecular speed following Maxwell distribution and d is the (cylindrical) pore diameter. After Knudsen's original work using straight tubes, researchers investigated the effects of pore structures and physico-chemical interactions between molecules and pore walls on the KD using theoretical and simulation approaches. To the best of our knowledge, it is generally accepted that a shorter tube has a higher KD coefficient and any structural variations from the straight, round cylindrical tube hampers the KD-limited gas transport except for diverging tubes and slots at the inlet (See next section for detailed review). Although KD has been widely used to explain gaseous transport in engineering processes using porous media, effects of pore structures on the KD were seldom studied in detail. To investigate effects of tube structures on transmission probabilities (TPs), we begin this article with a brief literature review of KD in terms of theoretical and simulation approaches.

2 Background

2.1 Practical

We are motivated to study the effects of pore geometry on the KD by Park et al. (2007) work where large cavities connected to each other (forming hourglass-type pore structures) contributed to high molecular transport rates. Polymer materials showing Brunauer–Emmett–Teller (BET) (1938) isotherms typically possess “throat and cavity” microporosity characteristics of activated carbon (Budd et al. 2005). Although KD is one of the transport mechanisms, specific research on effects of pore structures on KD has not been fully investigated.

Membrane filtration includes various processes for liquid and gas separation. Recently, MD was closely examined because of the high selectivity and reuse of waste heat to increase feed temperature 40–70°C below the boiling point of water. Water molecules evaporate at the pore inlet, migrate through the membrane pore (tube-type), and condense at the permeate side in the direct contact MD (Zhang et al. 2012). The transport of water vapor through the pore is governed by three mechanisms: viscous flow, KD, and Brownian motion. The viscous flow is often found to be negligible (Lawson and Lloyd 1996), and Knudsen and Brownian diffusions are competing against each other depending on ambient pressure and temperature (Qtaishat et al. 2008). The total diffusivity of water vapor is proposed to be a superposition of the two diffusion mechanisms (Bosanquet 1944) such as

$$D_{\text{eff}}^{-1} = D_{\text{B}}^{-1} + D_{\text{K}}^{-1} \quad (1)$$

For dilute gases, temperature dependences are $D_{\text{B}} \propto T$ and $D_{\text{K}} \propto \sqrt{T}$. The square-root dependence of D_{K} on T is because the mean molecular speed is proportional to \sqrt{T} , following Maxwell's distribution (Reif 1965).

The KD is classified in terms of Knudsen number, Kn ($\equiv \lambda/d$), defined as the mean free path (λ) divided by the pore diameter (Karniadakis and Beskok 2002), which are $Kn < 10^{-3}$ for the continuum flow regime; $10^{-3} < Kn < 10^{-1}$ for the slip flow regime; $10^{-1} < Kn < 10^{+1}$ for the transition flow regime; and $10^{+1} < Kn$ for the free molecular flow regime where the Knudsen transport is noticeably influenced by pore geometry. In-depth research on gaseous slip flow with respect to the Knudsen number can be found for free-convection (Haddad et al. 2005, 2006), forced-convection (Haddad and Abuzaid 2006), and periodic oscillating gas flows (Haddad et al. 2007) in microchannels filled with porous media. As the Knudsen number increases in the slip flow regime, the Brownian diffusion becomes insignificant, and pore structure may strongly influence local mass transport.

Equation 1 implies that each diffusivity can be superpositioned to estimate the effective diffusivity. In molecular dynamics or Brownian dynamics (Ermak and Mccammon 1978; Allen and Tildesley 1987), several diffusion mechanisms can be implemented, and overall phenomena can be mimicked. A temperature gradient can exist along membrane pores, but the mean temperature is often used to estimate the effective diffusivity and derive analytic solutions of the permeate flux (Curcio and Drioli 2005; Qtaishat et al. 2008). Since the temperature dependencies of Brownian and Knudsen diffusions are already known, the temperature can be fixed at a reference point to investigate diffusivity variations due to pore geometry.

In this work, we used analytic derivations of the standard diffusion theory, numerical solutions of the integral equation theory (IET), and Monte Carlo (MC) simulations to investigate the TP as influenced by pore geometry. For a simplified system consisting of low-pressure gas, we assumed the following: (1) The system already reached thermal equilibrium with a constant temperature. (2) Momentum transport is negligible because the viscous effects are proven to be less important than diffusion in MD processes (Lawson and Lloyd 1996). (3) Collisions between molecules and tube walls are elastic so that momentum and energy are locally conserved. (4) The gas concentration is low enough to confirm that the mean free path (λ) is much larger than the pore diameter (d): in mathematical form, $\lambda \rightarrow \infty$ and so Kn ($\equiv \lambda/d$) $\rightarrow \infty$, where Kn is called the Knudsen number. (5) Other transport mechanisms such as Brownian diffusion, adsorption, and surface migration are negligible.

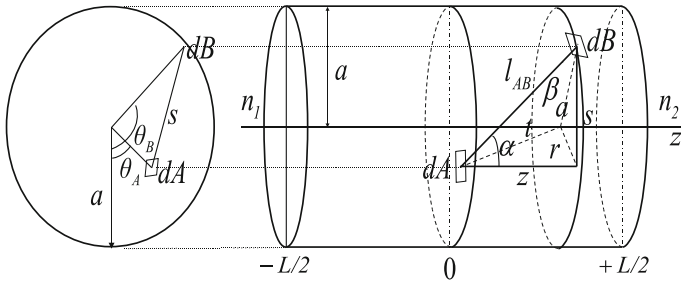


Fig. 1 Schematic of straight round cylindrical tube of length L and radius a . Clausing (1932, 1971) and Pollard and Present (1948) used axial ranges of $0 < z < L$ and $-L/2 < z < +L/2$, respectively

2.2 Theoretical

In Knudsen’s early work, the number of molecules of mass m and average velocity \bar{v} , passing through a given cross section of the straight tube of radius a per unit time, was given as $N_w = -\frac{16\pi a^2}{3m\bar{v}} \frac{dp}{dz}$, which was experimentally verified by Knudsen for low molecular concentrations with the pressure gradient along the tube dp/dz . One can define the molecular flux J as the ratio of N_w to the tube cross-sectional area of radius r_0 : $J = \frac{N_w}{\pi r_0^2} = -D_K \frac{dn}{dz}$ where dn/dz is the gradient of the molecular concentration along the tube of length L . The TP η is defined here as fraction of molecules that entered the (left) inlet of a tube, and exited at the (right) outlet without returning to the (left) reservoir, as shown in Fig. 1, i.e., $\eta = N_{out}/N_{in} = J_{out}/J_{in}$. In general, η is related to the Knudsen diffusivity as

$$\eta = \frac{D_K}{\frac{1}{4}\bar{v}L} = \frac{N/\pi a^2}{\frac{1}{4}\bar{v}L(-dn/dz)} \tag{2}$$

Clausing (1932, 1971) formulated rigorous mathematical representations of the direct and indirect TPs. The direct TP is a fraction of incoming molecules that pass through the tube without any collision with the tube wall, which is dominant for short tubes. Walsh (1919) developed a light radiation theory and calculated a fraction of the whole radiation flux from the first disk which falls on the second disk. The two coaxial disks of the same diameter, facing each other in parallel (as shown in Fig. 3 of Walsh’s 1919 work), are geometrically equivalent to the inlet and outlet cross sections, of the straight cylindrical tube. Clausing adopted Walsh’s solution as the direct TP, and developed the self-consistent IET to calculate the indirect TP, i.e., the fraction of molecules entering the inlet exit with at least one collision with the tube wall. The IET intrinsically dealt with the conditional probability that, given a molecule colliding with the tube wall at a location $0 < z < L$, the next random flight of the molecule from the collision point leads to the molecule’s escape at the tube outlet. When the tube length is much longer than the radius, i.e., $L \gg a$, the pressure inside the tube can be approximated as $p = \frac{1}{8}\pi nm\bar{v}^2$. Using Eq. 2, Knudsen’s indirect TP is calculated as $\eta_{ind}^K = 4d/3L$, as an equivalent dimensionless form of D_K . Clausing however failed to give the asymptotic limit of η_{ind}^K for a long tube ($L \gg d$), but gave only the half the original expression, i.e., $\eta_{ind}^{C,Asym} = 2d/3L$. The direct TP for a long tube, $\eta_{dir}^{W,Asym} = d^2/4L^2$ (which we derived from Walsh’s work) seems to be negligible, but it must play a role when combined with the same order correction of the indirect TP.

Table 1 Summary of direct, indirect, and total TP expressions. In this work, $\eta_{\text{ind}}^{\text{PP}}$ and $\eta_{\text{dir}}^{\text{PP}}$ are recalculated using PP’s formalism by taking the difference between total and indirect TP, respectively

	Direct TP	Indirect TP	Total TP
Knudsen	Neglected	$\eta_{\text{ind}}^{\text{K}} = 4d/3L$	$\eta_{\text{tot}}^{\text{K}} \approx \eta_{\text{ind}}^{\text{K}}$
Walsh	Eq. 4 ($\eta_{\text{dir}}^{\text{W}}$)	–	–
Clausing	$\eta_{\text{dir}}^{\text{C}} = \eta_{\text{dir}}^{\text{W}}$	$\eta_{\text{ind}}^{\text{C}} = \int \omega_{sr}(x) w(x) dx$ $\eta_{\text{ind}}^{\text{C,Asym}} = \frac{2d}{3L} \neq \eta_{\text{ind}}^{\text{K}}$	$\eta_{\text{dir}}^{\text{C}} + \eta_{\text{ind}}^{\text{C}}$
PP	$\eta_{\text{dir}}^{\text{PP}} = \eta_{\text{tot}}^{\text{PP}} - \eta_{\text{ind}}^{\text{PP}}$	$\eta_{\text{ind}}^{\text{PP}} = \frac{3d}{4L} \left(1 - \frac{3d}{2L}\right)$	$\eta_{\text{tot}}^{\text{PP}} = \frac{3d}{4L} \left(1 - \frac{4d}{3L}\right)$
TW	–	–	$\eta_{\text{tot}}^{\text{TW}} \approx \eta_{\text{tot}}^{\text{C}}$
SKL	$\eta_{\text{dir}}^{\text{C}} = \eta_{\text{dir}}^{\text{W}}$	$\eta_{\text{ind}}^{\text{SKL}}$ (derived Eq. 8)	$\eta_{\text{dir}}^{\text{C}} + \eta_{\text{ind}}^{\text{SKL}}$

Pollard and Present (PP) (1948) approximated the Knudsen diffusivity for self-diffusing molecules in a pure gas at a uniform pressure gradient in a long capillary tube. As shown in Fig. 1, the planar symmetry was set up at the center of the tube ($z = 0$), and the tube inlet and outlet are located at $z = -L/2$ and $+L/2$, respectively. Net molecular flux was assumed to be invariant through the tube in the steady state, and calculated across the tube cross section at the center ($z = 0$) as a superposition of forward and backward fluxes along the positive and negative z -directions, respectively. Two fractions of molecules that enter the central cross section (at $z = 0$) after the last collision with the tube wall and a neighboring molecule were individually calculated and added afterward. Various cases of $d (=2a)$, L , and λ were investigated using the Boltzmann factor, $e^{-r'/\lambda}$, assigned as a probability that a molecule of the mean free path λ travels a distance r' after the last collision. PP’s theory provided the first-order correction as $\eta_{\text{tot}}^{\text{PP}} = \frac{3d}{4L} \left(1 - \frac{4d}{3L}\right)$ from Knudsen’s original work with the proper asymptotic behavior. Effects of the linear concentration on the KD coefficient through λ was studied later by Flory and Cutler (1993).

It is worthwhile to compare Clausing’s and PP’s theoretical approaches as they are partially contradictory to each other. Clausing’s IET dealt with all the possible collision events of exiting molecules in the past and provided an accurate numerical solution of the indirect TP, but failed to reach the asymptotic limit of the indirect TP for a long tube. On the other hand, PP’s theoretical framework was based on the symmetric axial coordinate z running from $-L'$ to $+L'$ where $L' (=L/2)$ is the half-length. Instead of adopting Walsh’s exact solution, PP calculated the direct TP at the tube center ($z = 0$) as a function of λ . Because PP did not individually derive direct and indirect TPs (but only total TP), we followed PP’s theory and separately recalculated the indirect TP as $\eta_{\text{ind}}^{\text{PP}} = \frac{4d}{3L} \left(1 - \frac{3d}{2L}\right)$ for an infinite λ and the direct TP $\eta_{\text{dir}}^{\text{PP}} = \eta_{\text{tot}}^{\text{PP}} - \eta_{\text{ind}}^{\text{PP}} = d^2/L^2$. Interestingly, $\eta_{\text{dir}}^{\text{PP}}$ is the fourfold asymptotic limit of Walsh’s exact solution, $\eta_{\text{dir}}^{\text{W,Asym}}$. PP’s direct TP deals with only a half-cylinder with length $L' (=L/2)$, which suggests a correction of PP’s direct TP by replacing L of $\eta_{\text{dir}}^{\text{PP}}$ with $2L'$. This discrepancy can be easily understood by Walsh’s setup of the two facing disks of equal size at distance L . PP calculated “net” flux through a circular cross section at the tube center ($z = 0$) from two half tubes of length $L/2$. As a summary, PP failed to reproduce Walsh’s solution of asymptotic direct TP for an infinite λ , but succeeded to update indirect TP for a long tube. For approximate solutions of KD with an infinite λ , it must be reasonable to take Walsh’s exact solution for the direct TP and use PP’s axial coordinate centered at $z = 0$, where $-L/2 < z < L/2$, to calculate appropriate analytic and/or perturbative solutions

for the indirect TP. Mathematical representations are organized in Table 1 and explained in Appendix A.1.

A dusty gas model was developed for gaseous diffusion through porous media under conditions of uniform (Evans III et al. 1961) and linear (Evans III et al. 1962) pressure profiles. Bosanquet's relationship of Eq. 1 was re-confirmed using uniform pressure. Porous media was modeled as stationary giant molecules, called dusty particles, and was characterized using macroscopic parameters of porosity and tortuosity without specific description of microscopic pore structures. For a constant pressure gradient, the net molecular flux of binary species was calculated using a linear concentration profile. In both articles, Evans III et al. (1961, 1962) assumed that the normal diffusivity is dependent on the gas concentration, and implied that the KD coefficient is independent of internal structures of porous media. Mason et al. (1967) further developed the dusty gas model to include effects of pressure and temperature gradient on KD phenomena. Present and DeBethune (1949) treated the viscous effects as a small additive perturbation on the binary gas flow at low pressure and reported that, in the Knudsen regime, the separation factor reaches a maximum. While studies described above are limited to straight cylindrical tubes or uniform porous media, Iczkowski et al. (1963) applied the theory of Clausing to diverging and converging conical orifices and found moderately good agreement with experimental observations. In-depth studies of KD phenomena through diverging and converging tubes and slots can be found elsewhere (Richley and Reynolds 1964; Reynolds and Richley 1964, 1967).

Recently, Bhatia and Nicholson (2011) examined the tortuosity for diffusion of light gases in nanoporous carbons using the Oscillator model of low-pressure transport which incorporated van der Waals attraction. They indicated that the direct use of the KD model to meso- or nano-scale pores is misleading due to inconsistencies arising from neglect of van der Waals forces. The Oscillator model developed by Bhatia et al. (2004) was specifically applied to methane transport in carbon slit pores by Lim and Bhatia (2011). Krishna and van Baten (2011) used molecular dynamics to investigate the concentration dependence of Fick's diffusivities for various gas species in cylindrical silica mesopores; and indicated that zero-loading diffusivity is consistently lower than the classical KD formula due to molecular adsorption on the pore surfaces. On the other hand, Ruthven et al. (2009) discussed the validity of the KD model by analyzing experimental permeance data for several light gases (He, Ar, N₂, CH₄, and C₃H₈) in a mesoporous silica membrane, and experimentally confirmed $D_K \propto \sqrt{T/M}$ where M is the molecular weight. Although these studies provided in-depth understanding of the KD at the molecular scale phenomena (molecular adsorption, surface diffusion, microscopic roughness of pore surfaces, and collision elasticity), pore geometries were all assumed to be straight cylinders or rectangular slots. Investigation of the KD influenced by pore geometry and periodicity is in a burgeoning stage. Here, we restrict our theory and simulations to the KD phenomena for $\lambda \gg d$ through micro- or meso-pores of various geometry without adsorption.

2.3 MC Simulation

Davis (1960) work was the first MC simulation to study effects of tube/pore structures on the TP. Pipe structures tested include a straight cylindrical tube, a cylindrical elbow, an annulus of two concentric cylinders, a straight cylindrical tube with restricted openings, and a straight cylindrical tube with restricted openings and a central blocking plate. All of the simulation results showed that the TPs are smaller than that of the straight cylindrical tube of the same length, calculated using the IET. Talley and Whitaker (1969) later MC study validated asymp-

otic TPs through sufficiently short and long straight round cylindrical tubes. After a molecule enters the inlet and collides with the tube wall, the direction of the next flight was randomly selected according to the microscopically rough wall surface, which provides directional deviation between incident and reflecting angles. The molecule moves in a direction until it reaches another location on the tube wall or permanently leaves the tube. Intermolecular collision is ignored due to the infinite mean free path (equivalently step size). The simulation algorithm was verified by checking that the total TP converges to 1 for very short tubes and $4d/3L$ for very long tubes. The Knudsen flow through a converging–diverging tube (similar to a hourglass) has been studied, and the results indicated that “significant reductions in the flow rate can occur for channels having the same average diameter but varying degrees of curvature in the direction of flow.” A representative tube dimension was chosen as the average radius along the hourglass-like converging–diverging tube. In our opinion, however, the root-mean-square of the varying radii (instead of the average radius) along the tube channel can provide a more meaningful representation of the equivalent (constant) radius to have an equal internal volume. (See next section for mathematical details.) Simulation studies so far concluded that any structural modification from the conventional cylinder noticeably reduces the TP per given length and void volume. Owing to mathematical complexity, analytic solutions are limited to simple geometries such as a straight cylindrical tubes with several perturbative variations only (Steckelmacher 1986).

3 Theory and Simulations

In this study, the equivalent diameter d_{eq} was calculated based on the internal volume per unit length:

$$d_{\text{eq}}^2 = \frac{4}{\pi} \frac{V}{L} = \frac{1}{L} \int_{-\frac{1}{2}L}^{+\frac{1}{2}L} d_p^2(z) dz \quad (3)$$

where $d_p(z)$ is the tube diameter as a function of the axial position z in cylindrical coordinates. The equivalent diameter of the straight (conventional) cylinder is equal to its diameter, i.e., $d_{\text{eq}} = d$. We only consider variation of diameters along the tube’s axis so that azimuthal symmetry still remains valid for all the cases to be discussed, and tube interiors are transparent along the straight epi-center from inlet to outlet.

3.1 Cylindrical Tube

As stated above, both Clausing’s and PP’s theories are not self-consistent in terms of asymptotic limits of very long and very short tubes, respectively. To fundamentally resolve this inconsistency, we revisit here the original theories of Walsh (1919), Clausing (1932, 1971), and Pollard and Present (1948), take mathematical advantages from each theory, and derive a novel analytic solution for the indirect TP, assuming the linear concentration profile. In addition, we individually calculate the direct and indirect TPs using MC simulations following Talley and Whitaker (1969) algorithm, and compare systematically total TP with other results in the literature. Methods used here will be extended to tubes of various structures in later sections.

Clausing’s solution for the direct TP (taken from [Walsh’s 1919](#) work) is

$$\eta_{\text{dir}}^{\text{C}} = \frac{\sqrt{L^2 + d^2} - L}{\sqrt{L^2 + d^2} + L} \tag{4}$$

which, for a sufficiently short tube ($L \ll d$), converges to $1 - 2L/d$ indicating the linear dependence of the direct TP on the dimensionless tube length, and for a very long tube ($L \gg d$) reaches $d^2/4L^2$ decreasing much faster than the indirect TP. Now, we develop an analytic solution of the indirect TP using PP’s mathematical framework with the following assumptions: (1) The molecular flow is in steady state, (2) The flow is purely molecular, i.e., there are only elastic collisions between molecules and the tube wall (i.e., no inter-molecular collisions), and (3) The molecule collisions with the tube wall are taken as if gas molecules are diffusively reflected so that their velocity directions follow the cosine law. These over-simplified assumptions are similar to those used in the literature, but our objective in this section is to correct Clausing’s and PP’s approaches using a universal framework. [Figure 1](#) shows a schematic of the Knudsen flow through a straight tube with an arbitrary length L and a diameter $d (=2a)$. The tube is connected to a reservoir at $z = -L/2$ containing molecules of a low concentration n_1 , and the flow through the tube does not disturb the equilibrium. At $z = +L/2$, vacuum conditions exist by setting $n_2 = 0$ (for simplicity), so that no flow is returning from this region to the tube interior. This setup originates from the fact that the KD coefficient with an infinite λ does not significantly depend on molecular concentration and pressure gradients, but only on the tube geometry. This theory deals with the net flux across the cross section so that an addition of an arbitrary concentration n_0 at each side of the tube does not change the theoretical results.

The number of molecules, dN_w , coming from an element dB of the tube wall and passing through an infinitesimal area dA at the tube center per unit time, is given as $-dN_w = n(z) \bar{v}(dA \cos \alpha) (dB \cos \beta)/4\pi l_{AB}^2$ using the classical kinetic theory ([Reif 1965](#)), where $n(z)$ is the number concentration at the position z , l_{AB} is the distance between dA and dB , and α and β are angles between l_{AB} and normal directions to dA and dB , respectively. The following geometrical relationships are used: $dA = r dr d\theta_A$, $dB = a dz d\theta_B$, $\cos \alpha = z/l_{AB}$, $\cos \beta = (l_{AB}^2 + a^2 - r^2) / 2al_{AB}$, $l_{AB}^2 = r^2 + a^2 - 2ra \cos(\theta_A - \theta_B) + z^2$, and $r^2 = r^2 + z^2$. Integrating $-dN_w$ over the central cross section and whole internal wall surfaces yields

$$-N_w = \frac{\bar{v}}{4\pi} \int_A dA \int_B dB n(z) \frac{z [a - r \cos(\theta_A - \theta_B)]}{[z^2 + a^2 + r^2 - 2ra \cos(\theta_A - \theta_B)]^2} \tag{5}$$

where $\int_A dA = \int_0^{2\pi} d\theta_A \int_0^a r dr$ and $\int_B dB = \int_0^{2\pi} d\theta_B \int_{-L/2}^{+L/2} dz$. In order to calculate N_w , $n(z)$ should be known. Following [Pollard and Present’s \(1948\)](#) work, we assume that the molecular concentration linearly decreases from the (left) inlet to the (right) outlet sections: $n(z) = \frac{n_1}{2} + \left(\frac{dn}{dz}\right) z$, which is substituted into [Eq. 5](#) to yield

$$-N_w = 2\bar{v}a \left(\frac{dn}{dz}\right) \int_0^a r dr \int_0^{L/2} dz \times \int_0^{2\pi} d\theta_A \int_0^{2\pi} d\theta_B \frac{z^2 [a - r \cos(\theta_A - \theta_B)]}{[z^2 + a^2 + r^2 - 2ra \cos(\theta_A - \theta_B)]^2} \tag{6}$$

where $dn/dz = -n_1/L$ is a constant, and the term of $n_1/2$ in the integral vanishes by symmetry. We consider the relative angle $\theta_{AB} = \theta_A - \theta_B$ and replace the integration with respect to θ_A by 2π . This is because a rotation of dA in the azimuthal direction in Fig. 1 does not change the result of the angular integration with respect to θ_B . In addition, due to the planar symmetry, integration over θ_B from 0 to π should be equal to that from π to 2π . For simplicity, we set $\theta = \theta_B + \pi$. Equation 6 is integrated with respect to θ from 0 to π and r from 0 to a :

$$N_w = \pi a^2 \nu \int_0^{L/2} \frac{1}{a^2} \left[\sqrt{z^2 + 4a^2} + \frac{z^2}{\sqrt{z^2 + 4a^2}} - 2z \right] \frac{z}{L} dz \quad (7)$$

where $\nu = \frac{1}{4} \bar{v} L \left(-\frac{dn}{dz}\right)$ is the incidence rate of gas molecules striking the tube wall. Integration of Eq. 7 over z for the half tube due to symmetry finally provides

$$\eta_{\text{ind}}^{\text{SKL}} \equiv \frac{N_w}{\pi a^2 \nu} = \frac{4}{3} \left(\frac{d}{L}\right) \left[1 - \frac{1}{4} \left(\frac{L}{d}\right)^3 + \frac{1}{4} \left(\left(\frac{L}{d}\right)^2 - 2\right) \sqrt{\left(\frac{L}{d}\right)^2 + 4} \right] \quad (8)$$

where superscript ‘‘SKL’’ indicates initials of the authors’ last names.

We also calculated the direct and indirect TPs through the conventional cylindrical tube using the MC method and reproduced results of Talley and Whitaker (1969), which should be identical to Clausing’s exact solutions. A fourth assumption to those in our theory (discussed above) is that (4) molecules have equal chance of entering at any inlet point of the tube, arriving with an orientation distribution according to the cosine law. The MC algorithm employs the following procedures:

1. A molecule is randomly positioned at the inlet circular cross section at $z = -L/2$, and its flight direction toward the tube interior is arbitrarily chosen. The molecular flux at the inlet cross section is proportional to the cosine of the incident angle.
2. If the molecule leaves the tube at $z = +L/2$ immediately after it passes the inlet, the number of the escape events increases by one; if the molecule collides with the tube wall at a point inside the tube ($-L/2 < z < +L/2$) on the wall ($r = d/2$), the next flight direction is randomly selected from the last collision point. This is based on the assumption that the tube wall is rough at the molecular length scale.
3. (a) If the next flight leads the molecule to return to the (left) reservoir, then it is canceled; if the next flight guides the molecule to escape from the tube at the (right) outlet, then the number of the escape events is increased by one. In both cases, the simulation procedure goes to Step 1 with a new molecule created at the tube inlet. (b) If the molecule reaches a new point on the tube wall, a random collision will decide a new arbitrary direction, and molecule-wall collisions continue until the molecule escapes at the tube outlet or returns to the (left) reservoir.
4. The number of molecules escaping from the tube divided by the total number of entering molecules provides the total TP, and a fraction of escaped molecules not colliding with the tube wall contributes to the direct TP. The difference between total and direct TP is the indirect TP.

Figure 2 compares the direct and indirect TPs of various theoretical approaches and our MC simulations (a reproduction of Talley and Whitaker’s 1969 work). Figure 2a shows that our MC simulation ($\eta_{\text{dir}}^{\text{SKL, MC}}$) and Clausing’s direct TP ($\eta_{\text{dir}}^{\text{C}}$) perfectly match each other, as also indicated for indirect TPs of the $\eta_{\text{ind}}^{\text{SKL, MC}}$ and $\eta_{\text{ind}}^{\text{C}}$ in Fig. 2b. The asymptotic form of

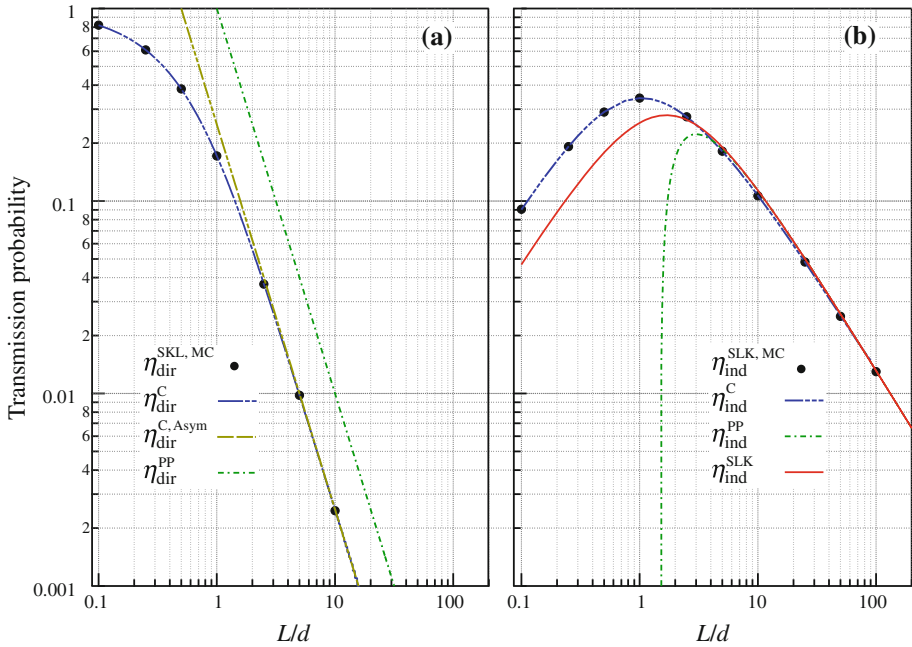


Fig. 2 Comparison of **a** direct and **b** indirect TPs versus dimensionless tube length L/d

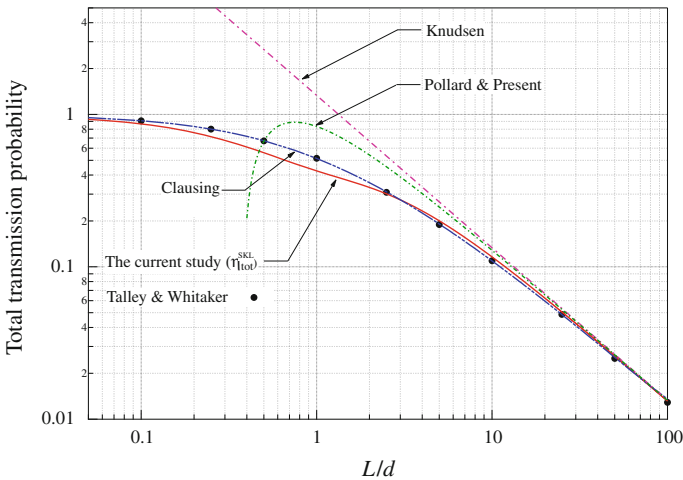


Fig. 3 Total TP versus dimensionless tube length L/d . Clausing (1932, 1971) IET and Talley and Whitaker (1969) MC simulations were reproduced by us. Equations used for Knudsen’s and Pollard & Present’s graphs are η_{ind}^K and η_{tot}^{PP} , respectively

Clausing’s direct TP ($\eta_{dir}^{C, Asym}$) agrees well with the exact solution η_{dir}^C for $L \gtrsim 2d$, and PP’s approximation of the direct TP (η_{dir}^{PP}) provides fourfold overestimation of $\eta_{dir}^{C, Asym}$. Figure 2b indicates that our analytic solution for the indirect TP (η_{ind}^{SLK}) is superior to that of the original PP’s theory (η_{ind}^{PP}), especially for short tubes.

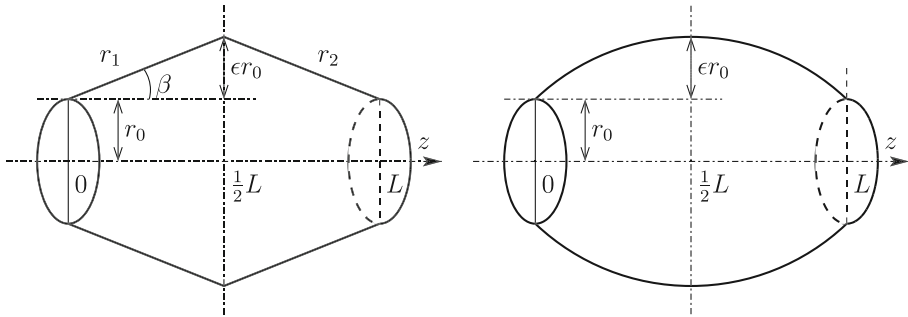


Fig. 4 Schematic of **a** a double conical and **b** bulging tubes

The total TP $\eta_{\text{tot}}^{\text{SKL}}$ is plotted in Fig. 3 and compared with Knudsen’s, Clausing’s, and PP’s theoretical results, and our MC simulations. As expected from results shown in Fig. 2, Clausing’s exact solution and the MC simulation agree very well, and our analytic solution provides closer approximation to Clausing’s exact solution than Knudsen’s and PP’s works. Theoretical/simulation results developed in this study are a marginal analytic development and a numerical reproduction of past research papers, respectively. However, analytic calculation of the closed form of Eq. 8 is not trivial as detailed derivation steps indicate. For a medium-length tube ($1 < L/d_{\text{eq}} < 10$), our analytic solution for the indirect tube significantly increases the accuracy for the total TP without requiring numerical solutions, and indicates that PP’s geometric setup provides physically unreasonable results due to the four fold error in the direct TP. In the next section, we will use the same approaches to investigate KD phenomena through tubes with various structures.

3.2 Diverging–Converging Tube

KD phenomena through converging, diverging, and converging–diverging tubes were previously scrutinized by Talley and Whitaker (1969). But, until now, similar research work is very rare, despite the scientific and engineering importance. To the best of our knowledge, the (conically) diverging–converging tube (as shown in Fig. 4a), such as two head-cut conical tubes connecting their wider mouths, was not investigated for gas transport in the Knudsen regime. Radii of the left and right sides of conical tubes are expressed as a function of the axial distance from the inlet:

$$r(z)_{\text{div-conv}} = \begin{cases} r_1 = r_0 + \epsilon \frac{2r_0}{L} z, & 0 \leq z \leq \frac{L}{2} \\ r_2 = r_0 + \epsilon \frac{2r_0}{L} (L - z), & \frac{L}{2} < z \leq L \end{cases} \quad (9)$$

and the magnitude of opening/closing angle β at the inlet/outlet is related to ϵ , i.e., the dimensionless distance from the imaginary tube surface of radius r_0 at the mid-point (at $z = L/2$) to the peak of the diverging–converging tube, $r_0 + \epsilon r_0: \tan \beta = 2\epsilon a/L$. From Eq. 3, the equivalent diameter of the diverging–converging tube is derived as

$$d_{\text{eq}}^{\text{div-conv}} = 2r_0 \sqrt{1 + \epsilon + \frac{1}{3} \epsilon^3} \quad (10)$$

Following the Clausing’s IET, we write the indirect TP as

$$\eta_{\text{ind}} = \int_0^L \omega_{sr}(z) w(z) dz \tag{11}$$

so that $\eta_{\text{tot}} = \eta_{\text{ind}} + \omega_{ss}(z)$ where $w(z)$ is the escape probability that the molecule currently at z will pass the (right) outlet without returning to the left reservoir, i.e.,

$$w(z) = \int_0^L \omega_{rr}(y-z) w(y) dy + \omega_{rs}(L-z) \tag{12}$$

Here, we used the following definitions as extended from Clausing’s work:

1. $\omega_{rr}(y)$ is the probability that a molecule, which in accordance with the cosine law leaves a ring within an infinitesimal area, $2\pi r(z) dz$ at z , strikes directly on another ring $2\pi r(z+y) dz$ located at a distance y from the first ring;
2. $\omega_{rs}(y)$ is the probability that a molecule leaving a ring $2\pi r(z) dz$ at z passes directly through a cross section at the distance $y (= L - z)$;
3. $\omega_{sr}(z)$ is the probability averaged over the inlet cross section πr_0^2 that a molecule leaving the section strikes directly on a ring $2\pi r(z) dz$ at a distance z ; and
4. $\omega_{ss}(z)$ is the probability, averaged over the inlet cross section πr_0^2 that a molecule entering the tube directly passes the outlet cross section at the distance $z (= L)$, which is identical to Eq. 4, i.e., Walsh’s analytic solution that Clausing adopted.

Specific analytic forms of ω -functions are included in Appendix A.2. We numerically solve the integral Eq. 11 after the self-consistent solution for $w(z)$ is obtained.

Figure 5 shows the total TP of the diverging–converging and bulging tubes calculated using our IET and MC simulations, compared with that of the equivalent straight tube. All three tubes have the same internal volume, and the equivalent radius is calculated as the root-mean-square of the radius $r(z)$. Unless the tube length is comparable to the diameter, the total TP of diverging–converging tube is noticeably higher than that of the equivalent straight tube. Davis (1960) reported the reduction in the total TP of the converging–diverging tube. This is because molecules entering the tube inlet must have a lower chance to pass through the tube due to the narrowing diameter towards the center. Our simulation results show that the center-widening tube provided higher TP than that of an equal-volume straight tube. Although the elastic molecular reflection on the tube wall is of random direction, the opening slope of the tube inlet allows molecules to reflect more toward the center of a diverging tube. If molecules bouncing off the (left half) inlet wall pass through the tube-outlet, they are directly transmitted from the inlet region to the outlet. This can be more probable in the diverging–converging tube than in the straight tube in terms of the pore geometry. Molecules colliding with the (right-half) outlet wall will be reflected more toward the center, which may reduced the effective TP, but this probability must be (almost) canceled out by the same influence from the inlet wall. The opening inlet structure not only pushes entering molecules toward the outlet, but also prevents molecules from returning to the reservoir. The net effect is represented as the enhanced TP through the diverging–converging tube. It is hard to prove this analysis using standard methods, and so we formulated a perturbation theory:

$$\eta_{\text{ind}}^{\text{div-conv}} = \eta_{\text{ind}}^{\text{SKL}} + \varepsilon f\left(\frac{L}{d}\right) + O(\varepsilon^2) \tag{13}$$

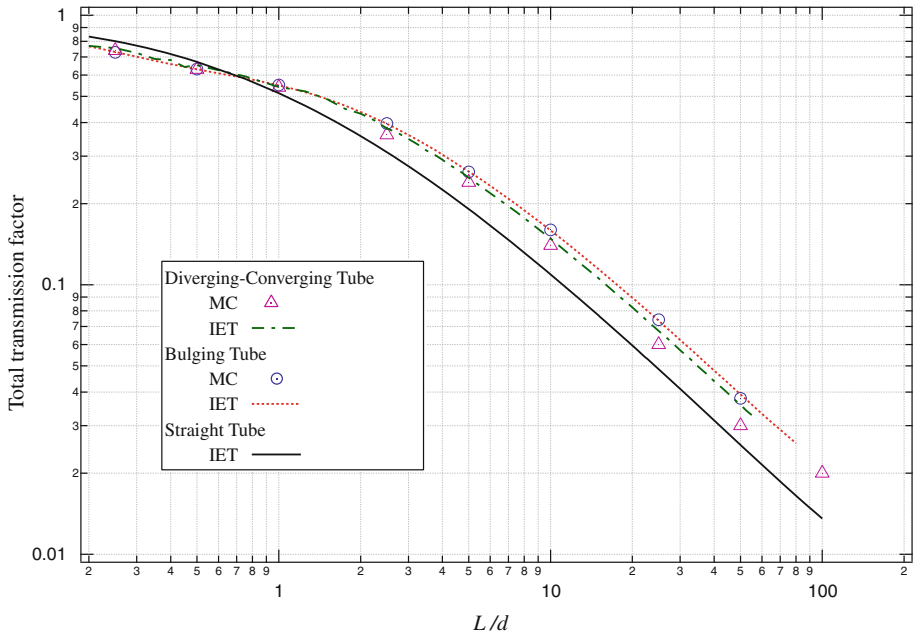


Fig. 5 Total TP of the diverging–converging and bulging tubes versus the dimensionless tube length (L/d) with $\varepsilon = 0.5$, calculated using the IET and MC simulations, as compared with Clausius’s exact solution. The equivalent diameters of the diverging–converging and bulging tubes are calculated using Eqs. 10 and 16, respectively

and calculated

$$f\left(\frac{L}{d}\right) = \frac{d}{L} \left[4 + \frac{L}{2d} + \frac{2d}{L} \ln\left(\frac{2d}{L + \sqrt{L^2 + 4d^2}}\right) - \frac{L^2 + 12d^2}{2d\sqrt{L^2 + 4d^2}} \right] \tag{14}$$

which converges to $f \rightarrow \frac{4d}{L}$ for $L \gg d$ and $f \rightarrow \frac{1}{2}$ for $L \ll d$. Scaling of L using d_{eq} (instead of $2r_0$) does not change the first-order correction of f with respect to L/d . Note that the sign of the perturbation function f is always positive. See Appendix A.3 for detailed calculations.

3.3 Bulging Tube

Now we investigate the molecular transmission through a bulging tube, which is a sinusoidally diverging–converging tube, as shown in Fig. 4b. The variation of radii along the axial coordinate from $z = 0$ to L is represented as

$$r(z)_{bulging} = a + \varepsilon a \sin\left(\frac{\pi z}{L}\right) \tag{15}$$

The indirect TP is numerically calculated using the Clausius’s IET of Eq. 11 and the direct TP is identical to Walsh’s solution (ω_{ss}). We analytically derived three other ω ’s for this bulging tube, which are included in Appendix A.4. The equivalent diameter of this bulging tube is calculated as

$$d_{eq}^{bulging} = 2r_0 \sqrt{1 + \frac{4}{\pi}\varepsilon + \frac{1}{2}\varepsilon^3} \tag{16}$$

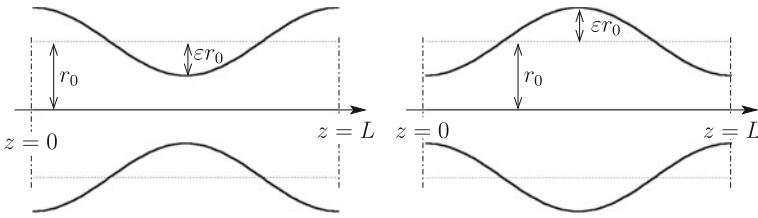


Fig. 6 Schematic of **a** positive and **b** negative cosinusoidal tubes. The pore shape was described by **a** $r(z) = r_0 + \epsilon r_0 \cos\left(\frac{2\pi z}{L}\right)$ and **b** $r(z) = r_0 - \epsilon r_0 \cos\left(\frac{2\pi z}{L}\right)$ with $m = 1$. Functions used in **a** and **b** have a phase difference of $L/2$ with respect to z

Owing to the geometric complexity of this bulging tube, an analytic solution is not available, and therefore only the MC simulations are performed. Figure 5 shows that the total TPs of the bulging tube is, in general, higher than that of the diverging–converging tube. Opening slopes of the two tubes are calculated by derivatives of Eqs. 9 and 15 with respect to z at $z = 0$:

$$\left[\frac{dr(z)_{\text{div-conv}}}{dz} \right]_{z=0} = \epsilon \frac{2r_0}{L} = \epsilon \frac{d_{\text{eq}}^{\text{div-conv}}}{L} \frac{1}{\sqrt{1 + \epsilon + \frac{1}{3}\epsilon^3}} \tag{17}$$

$$\left[\frac{dr(z)_{\text{bulging}}}{dz} \right]_{z=0} = \epsilon \left(\frac{\pi}{2}\right) \frac{2r_0}{L} = \epsilon \frac{d_{\text{eq}}^{\text{bulging}}}{L} \frac{\pi/2}{\sqrt{1 + \frac{4}{\pi}\epsilon + \frac{1}{2}\epsilon^3}} \tag{18}$$

The ratio of Eqs. 18 to 17 indicates that for small ϵ , the bulging tube has an inlet slope as much as $\pi/2$ times as higher than that of the diverging–converging tube with the same equivalent diameter. This implies that the geometrical slope at the inlet noticeably increases the total transmission factor as compared to that of the equivalent straight tube. For filtration processes, the pore sizes should be small enough to reject solute ions or particles, but larger void spaces that provide opening slopes at the pore inlet can enhance the solvent transport through membranes. To address these phenomena, the free volume theory is readily accepted to investigate gas transport through polymer membranes (Mulder 1996).

3.4 Periodic Tube

TP of periodic tubes is investigated using only the MC method for pore structures which are divided into two groups, positive and negative cosinusoidal tubes, as described by

$$r(z)_{\text{periodic}} = r_0 \pm \epsilon r_0 \cos\left(\frac{2m\pi z}{L}\right) \tag{19}$$

where m is the periodicity coefficient. Figure 6 shows the pore structures of $m = 1$ and $\epsilon = \pm 0.5$. The tube slope at the inlet is zero because the cosine function has a maximum and minimum at every half-period, $L/2$. The equivalent diameter of this periodic tube (independent on the periodicity coefficient m) is given as

$$d_{\text{eq}}^{\text{periodic}} = 2r_0 \sqrt{1 + \frac{1}{2}\epsilon^2} \tag{20}$$

which indicates that the equivalent diameter is (slightly) greater than $2r_0$. The second order of ϵ has only a minimal influence. We calculate the inlet slope at the first location where the

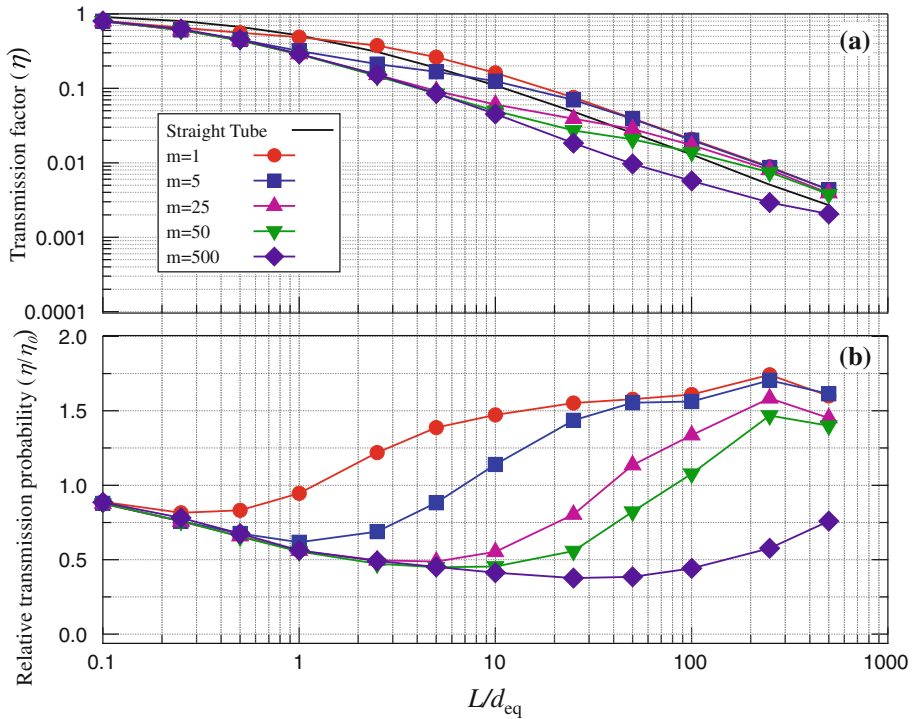


Fig. 7 Total TP of a periodic, negative cosinusoidal tube with $\varepsilon = 0.5$ versus the dimensionless tube length L/d_{eq} : **a** log–log and **b** semi-log plots

tube radius is equal to the base line of the tube at $z = L/4m$ as

$$\left[\frac{dr(z)_{\text{periodic}}}{dz} \right]_{z=L/4m} = \pm \varepsilon r_0 \frac{2m\pi}{L} = \pm \varepsilon \frac{d_{eq}^{\text{periodic}}}{L} \frac{m\pi}{\sqrt{1 + \frac{1}{2}\varepsilon^2}} \quad (21)$$

so that, as m increases, the diverging/converging slope of the positive/negative cosinusoidal tube increases in magnitude accordingly. Davis (1960) implied that narrower centers (than inlets and outlets) decrease the transmission factor. We simulated the TPs for both positive and negative cosinusoidal tubes. The TP of a positive cosinusoidal tube always gives smaller TPs than those of the equivalent tube (See Appendix A.5 for details). Figure 7 shows the total TPs of the negative cosinusoidal tubes versus L/d_{eq} with $\varepsilon = 0.5$. Since we used integer m values of 1, 5, 25, 50, and 500, the equivalent diameters in Fig. 7 are all identical. As m increases, the crossing point is farther from the tube inlet. Although advanced probabilistic analysis is required to understand these interesting phenomena, we analyze our findings as follows. If $m = 0$, the radius is constant as $r(z) = r_0(1 \pm \varepsilon)$ indicating straight tubes. If m is very large, a peak-to-peak distance (i.e., L/m) is much smaller than the tube diameter. Here, the peak indicates regions where the tube is locally bulged, i.e., near $z = (L/m)n$ for $1 \leq n \leq m - 2$ of the positive cosinusoidal tube, and $z = (L/m)(n + \frac{1}{2})$ for $1 \leq n \leq m - 1$ of the negative cosinusoidal tubes. As m increases, the spatial period L/m becomes negligible in comparison to r_0 . In this case, molecules cannot easily fly into the peak zones. If molecules enter the narrow regions, then they must stay in the locally confined zones for a

long time and hence cannot easily pass through the tube. In either case, the effective tube radius can be considered as $r_0 - \varepsilon$. If the value of m is finite and close to L/d_{eq} , then the bulging central zone within each period is considered to enhance the Knudsen transport. In our opinion, the opening inlet of each period enhances the molecular transport (as discussed in Sect. 3.2). When molecules are reflected backward from the exit to the inlet side in each spatial period, the diverging inlet plays a similar role to the converging outlet in a way that the inlet geometry partially prevents the backward molecular flight to the previous spatial period, keeping molecules inside the specific spatial period and pushing them more toward the exit side. Because our approach is one of equilibrium simulations, which focuses on the time-averaged probability, further investigation is required using a time-evolution simulation such as molecular dynamics (Allen and Tildesley 1987). It is, however, interesting to observe in Fig. 7a that each TP curve with specific m crosses that of the equivalent straight tube, and that the crossing points measured as L/d_{eq} are very close to the periodicity coefficient m (specifically for $\varepsilon = 0.5$). Figure 7b clearly shows this trend: the crossing points of $m = 1, 5, 25,$ and 50 are roughly estimated as $L_{\text{cross}}/d_{\text{eq}} = 1.1, 7.0, 40,$ and $80,$ respectively. The MC simulations for $L/d \geq 1,000$ took an unreasonably long time (more than a few weeks), but the general trend of Fig. 7b for $m = 500$ indicates that the ratio can exceed 1.0 near $L/d = 1,000$. Comparing the total TPs of the positive and negative cosinusoidal tubes implies that the pore structure at the tube inlet significantly influences the Knudsen transport through the long tubes.

Figure 7 (and Fig. 9 in Appendix A.5) provides significant engineering implications. First, it is generally understood (in the literature) that any structural changes from the conventional straight, round cylindrical tube hamper the Knudsen transport by effectively blocking molecular movements from the inlet to the outlet with the only exception of tubes having diverging–converging structure from the inlet ($z = 0$). If a periodicity characterized by m is implemented in the tube radius along the length, then the TP of the periodic tube exceeds that of the equivalent straight tube near $L_{\text{cross}}/d_{\text{eq}}$ or after. A higher amplitude of the periodicity, ε , increases the TP of the periodic tube as much as 1.6 times, estimated visually from Figs. 7 and 9; but the trade-off is a longer dimensionless crossing distance $L_{\text{cross}}/d_{\text{eq}}$ at which the TP ratio becomes unity. The optimal geometry for the maximum TP seems to be dependent on the dimensionless tube length; however, if the periodicity coefficient is about an order of magnitude less than the dimensionless tube length, then the relative TP reaches its maximum value. From Figs. 7b and 9b (for cases of $m = 1$ and 5), the maximum TP ratios are roughly estimated as 1.7 and 1.6, respectively.

4 Conclusions

In this study, we investigated the direct and indirect TPs through various tube structures using the standard diffusion theory, IET, and MC simulations. We derived an analytic solution for the indirect TP using the standard diffusion theory, with which Walsh's exact solution provides a complete solution set for the total TP through a conventional cylindrical tube. The diverging tube with the opening inlet structure noticeably enhances the indirect TPs, and the bulging tube which has a stiffer opening slope gives a higher TP than that of the diverging–converging tube of the same void volume. Periodic tubes show a higher TP than that of the equivalent tube as the dimensionless length exceeds the periodicity coefficient depending on the tube peak-amplitude. We also found that the framework of the axial range in the cylindrical coordinates influences the asymptotic representations of the TPs.

Acknowledgements This research was supported by a grant from the US National Science Foundation Faculty Early Career (CAREER) Development Program (CBET04-49431) and the International Scholar Program of Kyung Hi University, Korea.

Appendix

A.1 Comparison of Theoretical Approaches

Table 1 summarizes the expressions of direct, indirect, and total TPs discussed here with asymptotic forms and mathematical methods used. Knudsen’s asymptotic solution for the indirect TP for a long tube and Walsh’s exact analytic solution for the direct TP provided the theoretical framework for further investigations. A complete solution was developed by Clausing’s IET, but its series expansion did not match η_{ind}^K . PP calculated only the total TP, and did not use Walsh’s exact solution. Clausing and PP failed to provide correct asymptotic limits of indirect and direct TPs, respectively, while Walsh’s solution for the direct TP remains rigorously valid. Talley and Whittaker confirmed Clausing’s complete solution using MC experiments. We calculated the analytic solution of indirect TP with the linear concentration assumption and proposed the analytic expression of the total TP as a superposition of our indirect TP and Walsh’s direct TP.

Probability Functions of the Diverging–Converging Tube

Mathematical expressions of probabilities from ring or section to (another) ring or section, ω ’s, in the conically diverging–converging tube are calculated as follows:

1. From section to section ω_{ss}

$$\omega_{ss}(L) = 1 - \frac{2L}{L + \sqrt{L^2 + 4r_0^2}}; \tag{22}$$

2. From section to ring ω_{sr}

$$\omega_{sr}\left(0 \leq z \leq \frac{1}{2}L\right) = \frac{1}{r_0^2} \left[\frac{\sec \beta (z^2 \sec^2 \beta + 3r_0z \tan \beta + 2r_0^2)}{\sqrt{z^2 \sec^2 \beta + 4r_0z \tan \beta + 4r_0^2}} - (z \sec^2 \beta + r_0 \tan \beta) \right], \tag{23}$$

$$\omega_{sr}\left(\frac{1}{2}L \leq z \leq L\right) = \frac{1}{r_0^2} \left[\frac{z (r_2^2 + z^2 + r_0^2) - r_2 \tan \beta (r_2^2 + z^2 - r_0^2)}{\sqrt{(r_2^2 + z^2 + r_0^2)^2 - 4r_0^2r_2^2}} - (z + r_2 \tan \beta) \right]; \tag{24}$$

3. From ring to section ω_{rs}

$$\omega_{rs}(L - z) = \frac{\cos \beta}{2r_2} \left[\frac{(L - z) (r_2^2 + (L - z)^2 + r_0^2) - r_2 \tan \beta (r_2^2 + (L - z)^2 - r_0^2)}{\sqrt{(r_2^2 + (L - z)^2 + r_0^2)^2 - 4r_0^2r_2^2}} \right]$$

$$- ((L - z) - r_2 \tan \beta) \Big] \quad \text{for } 0 \leq z \leq \frac{L}{2}; \tag{25}$$

$$\omega_{rs}(L - z) = \frac{\cos \beta}{2r_2} \left[\frac{\sec \beta ((L - z)^2 \sec^2 \beta + 3r_0(L - z) \tan \beta + 2r_0^2)}{\sqrt{(L - z) \sec^2 \beta + 4r_0(L - z) \tan \beta + 4r_0^2}} \right. \\ \left. - ((L - z) \sec^2 \beta + r_0 \tan \beta) \right] \quad \text{for } \frac{L}{2} \leq z \leq L; \tag{26}$$

4. From ring to ring ω_{rr}

(a) For $0 \leq y, z \leq \frac{1}{2}L$ or $\frac{1}{2}L < y, z \leq L$

$$\omega_{rr}(y - z) = \frac{\cos \beta}{2r_z} \left[1 - \frac{|y - z| \sec \beta ((y - z)^2 \sec^2 \beta + 6r_z r_y)}{\sqrt{((y - z)^2 \sec^2 \beta + 4r_z r_y)}} \right]; \tag{27}$$

where

$$r_z = \begin{cases} r_0 + \frac{2\alpha r_0}{L} z, & 0 \leq z \leq \frac{L}{2} \\ r_0 + \frac{2\alpha r_0}{L} (L - z), & \frac{L}{2} < z \leq L \end{cases}$$

$$r_y = \begin{cases} r_0 + \frac{2\alpha r_0}{L} y, & 0 \leq y \leq \frac{L}{2} \\ r_0 + \frac{2\alpha r_0}{L} (L - y), & \frac{L}{2} < y \leq L \end{cases}$$

(b) For $0 \leq y \leq \frac{1}{2}L < z < L$ or $0 \leq z \leq \frac{1}{2}L < y < L$

$$\omega_{rr}(y - z) = 2r_y \cos \beta \left[\frac{b_0 d_0}{f_0^2} \left(1 - \frac{e_0}{\sqrt{e_0^2 - f_0^2}} \right) \right. \\ \left. + \frac{e_0(a_0 c_0 + b_0 d_0) - f_0(a_0 d_0 + b_0 c_0)}{(e_0^2 - f_0^2)^{3/2}} \right] \tag{28}$$

where $a_0 = r_z + |y - z| \tan \beta$, $b_0 = r_y$, $c_0 = r_y + |y - z| \tan \beta$, $d_0 = r_z$, $e_0 = x^2 + r_z^2 + r_y^2$, and $f_0 = 2r_z r_y$.

A.2 Perturbation Approach

In this section, we briefly describe how to obtain the perturbation solution for the indirect TP of the diverging–converging tube. Using a method similar to Walsh (1919) formalism, we consider two surface elements: one on the central cross section and another on the tube wall, denoted as dA and dA' , respectively. The normal direction of dA (and dA') has an angle θ

(and θ') with respect to the z -axis so that the relative angle between normal directions of dA and dA' is defined as $\phi = \theta - \theta'$. The distance of dA (and dA') from the z -axis is r (and r'). In this case, geometrical relationships are as follows:

$$dA = r \, dr \, d\theta \tag{29}$$

$$dA' = \frac{r' \, dz \, d\theta'}{\cos \beta} \tag{30}$$

$$\cos \phi = \frac{z}{l} = \frac{l^2 + s^2 - t^2}{2ls} \tag{31}$$

$$l^2 = r^2 + r'^2 - 2rr' \cos \phi + z^2 \tag{32}$$

$$t^2 = r^2 + (|z| - r' \tan \beta)^2 \tag{33}$$

$$s = \frac{r'}{\cos \beta} \tag{34}$$

$$r' = r_0 + \left(\frac{L}{2} - |z| \right) \tan \beta \tag{35}$$

which are used to calculate the infinitesimal number of molecules passing the central cross section per unit time:

$$-dN_w = n(z) \bar{v} \frac{(dA \cos \phi) (dA' \cos \phi)}{4\pi l^2} \tag{36}$$

where l is the distance between dA and dA' . The specific integral form of Eq. 36 is

$$-N_w = \frac{\bar{v}}{4\pi} \int_0^{2\pi} d\theta \int_0^{r_0(1+\varepsilon)} r \, dr \int_0^{2\pi} d\phi \int_{-\frac{1}{2}L}^{+\frac{1}{2}L} dz \, n(z) \frac{zr' (r' - r \cos \phi + |z| \tan \beta)}{(r^2 + r'^2 - 2rr' \cos \phi + z^2)^2} \tag{37}$$

where the integration with respect to θ gives 2π . After substituting the linear concentration profile into Eq. 37, we nullified the part of the integration having the constant term ($n_1/2$) of the concentration profile due to symmetry. Approximating $\tan \beta = \varepsilon r_0/h \approx \beta$ for small ε , we calculated the indirect TP of the diverging-converging tube as a perturbation series in terms of ε . The first-order approximation gives

$$\eta = \eta + \varepsilon f(h) \tag{38}$$

where the perturbation function is calculated as

$$f(h) = \frac{1}{h} \left[4 + \frac{h}{2} + \frac{2}{h} \ln \left(\frac{2}{h + \sqrt{h^2 + 4}} \right) - \frac{h^2 + 12}{2\sqrt{h^2 + 4}} \right] \tag{39}$$

where $h = L/2r_0 = L/d$ is the dimensionless length, i.e., the half-length divided by the radius of the diverging-converging tube.

A.3 Probability Functions of the Bulging Tube

Mathematical expressions of probabilities from ring or section to (another) ring or section, ω 's, in the bulging (sinusoidally diverging–converging) tube are calculated as follows:

1. $\omega_{ss}(z)$ is identical;
2. $\omega_{sr}(z)$
 - (a) $0 < z < L$

$$\omega_{sr}(z) = \frac{1}{r_0^2} \left[\frac{z(r^2 + z^2 + r_0^2) - r \tan \beta (r^2 + z^2 - r_0^2)}{\sqrt{(r^2 + z^2 + r_0^2)^2 - 4r_0^2 r^2}} - (z + r \tan \beta) \right], \tag{40}$$

where $\tan \beta = \frac{\alpha r_0 \pi}{L} \cos \frac{\pi z}{L}$.

- (b) $z = 0$

$$\omega_{sr}(0) = \frac{1}{r_0} \left\{ \left[1 + \left(\frac{\pi \alpha r_0}{L} \right)^2 \right]^{1/2} - \frac{\pi \alpha r_0}{L} \right\}; \tag{41}$$

3. $\omega_{rs}(L - z)$
 - (a) $0 < z < L$

$$\omega_{rs}(L - z) = \frac{\cos \beta}{2r} \left[\frac{(L - z)(r^2 + (L - z)^2 + r_0^2) - r \tan \beta (r^2 + (L - z)^2 - r_0^2)}{\sqrt{(r^2 + (L - z)^2 + r_0^2)^2 - 4r_0^2 r^2}} - ((L - z) - r \tan \beta) \right], \tag{42}$$

- (b) $z = L$

$$\omega_{sr}(0) = \frac{\cos \beta}{2} \left\{ \left[1 + \left(\frac{\pi \alpha r_0}{L} \right)^2 \right]^{1/2} - \frac{\pi \alpha r_0}{L} \right\}; \tag{43}$$

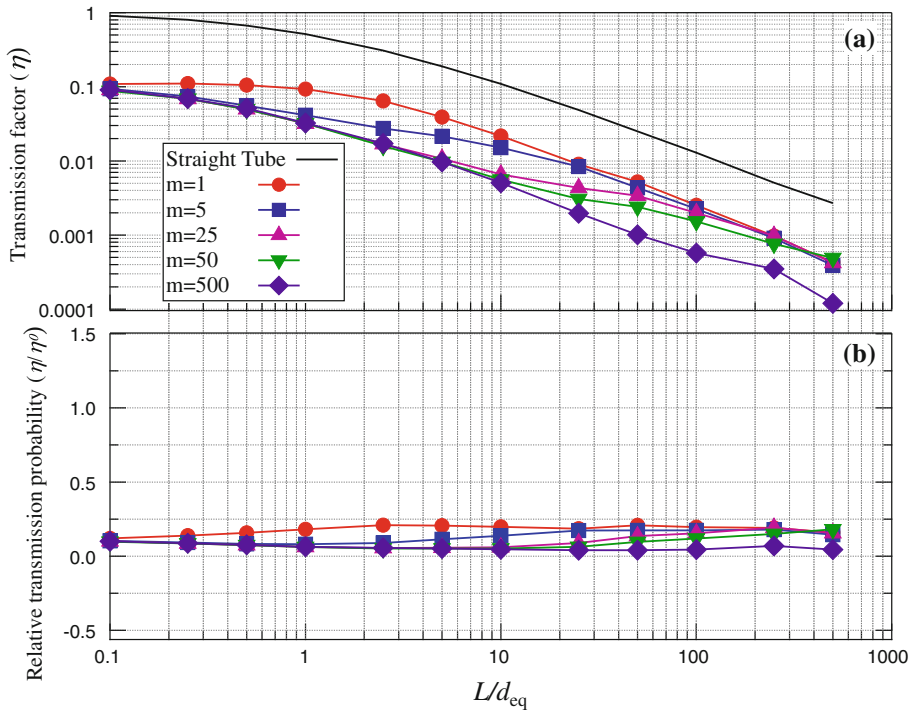


Fig. 8 Total TP of a periodic, positive cosinusoidal tube with $\varepsilon = 0.5$ versus the dimensionless tube length L/d_{eq} : **a** log–log and **b** semi-log plots

4. $\omega_{rr}(y - z)$

(a) $z \neq y$

$$\omega_{rr}(y - z) = 2r_y \cos \beta_z \left[\frac{b_0 d_0}{f_0^2} \left(1 - \frac{e_0}{\sqrt{e_0^2 - f_0^2}} \right) + \frac{e_0(a_0 c_0 + b_0 d_0) - f_0(a_0 d_0 + b_0 c_0)}{(e_0^2 - f_0^2)^{3/2}} \right]; \quad (44)$$

where $a_0 = r_z + |y - z| \tan \beta_z$, $b_0 = r_y$, $c_0 = r_y + |y - z| \tan \beta_y$, $d_0 = r_z$, $e_0 = x^2 + r_z^2 + r_y^2$, $f_0 = 2r_z r_y$, $r_z = a + \alpha a \sin \frac{\pi z}{L}$, $\tan \beta_z = \frac{\pi \alpha a}{L} \cos \frac{\pi z}{L}$, $r_y = a + \alpha a \sin \frac{\pi y}{L}$, and $\tan \beta_y = \frac{\pi \alpha a}{L} \cos \frac{\pi y}{L}$

(b) $z = y$

$$\omega_{rr}(0) = \frac{\cos \beta_z}{2r_z}. \quad (45)$$

A.4 TPs of the Periodic Tubes

The TPs of the positive cosinusoidal tubes are investigated using MC simulations with various periodicity coefficient values as used for the negative cosinusoidal tubes. Specifically, Fig. 8a

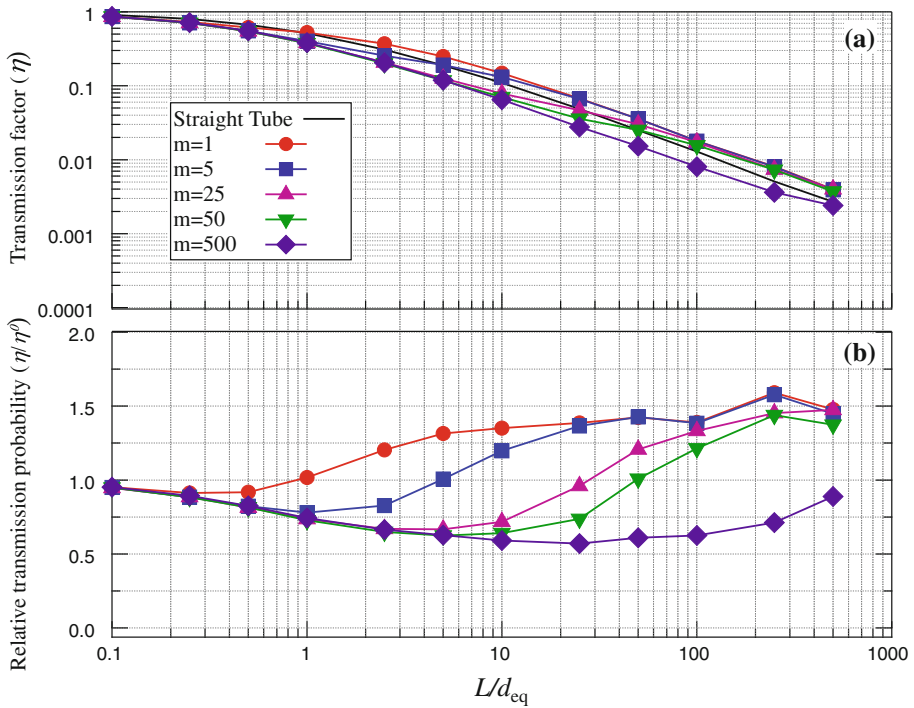


Fig. 9 Total TP of a periodic, negative cosinusoidal tube with $\varepsilon = 0.25$ versus the dimensionless tube length L/d_{eq} : **a** log–log and **b** semi-log plots

shows the total TPs for $\varepsilon = 0.5$ with m values of 1, 5, 25, 50, and 500. Except for the large $m = 500$, most of TPs look converging to that of $m = 1$ for long tubes $L/d_{eq} \geq O(10^2)$. As the solid line indicates the total TP of the equivalent tube, TPs of finite $m (\geq 1)$ are all below that of the equivalent tube. In addition, Fig. 8b indicates that the total TPs of the positive cosinusoidal tubes are about one order of magnitude smaller than that of the equivalent tube. We also did some MC simulations with $\varepsilon = 0.25$ so that the negatively cosinusoidal tubes have less geometric curvature on the lateral side than that of tube with $\varepsilon = 0.5$. Simulation results are shown in Fig. 9a, b for log–log and semi-log plots, respectively. Figure 9a shows the identical trend to that of Fig. 7a, but the TP curves of various m values are closer to that of the equivalent straight tube, which results in shorter crossing points after which the TPs of the negatively cosinusoidal tubes exceed that of the equivalent straight tube. For $m = 1, 5, 25,$ and $50, L_{cross}/d_{eq}$ values are roughly estimated from the ratio plot of Fig. 9b as 0.9, 5, 22, and 50, which are smaller than the corresponding values of the $\varepsilon = 0.5$ case, but surprisingly close to the m values used.

References

Allen, M.P., Tildesley, D.J.: Computer Simulation of Liquids. Oxford University Press, Oxford (1987)
 Bhatia, S., Nicholson, D.: Some pitfalls in the use of the Knudsen equation in modelling diffusion in nanoporous materials. Chem. Eng. Sci. **66**(3), 284–293 (2011)

- Bhatia, S.K., Jepps, O., Nicholson, D.: Tractable molecular theory of transport of Lennard–Jones fluids in nanopores. *J. Chem. Phys.* **120**(9), 4472 (2004)
- Bosanquet, C.H.B.: British TA Rept, pp BR–507 (1944)
- Brunauer, S., Emmett, P.H., Teller, E.: Adsorption of gases in multimolecular layers. *J. Am. Chem. Soc.* **60**(2), 309–319 (1938)
- Budd, P.M., McKeown, N.B., Fritsch, D.: Free volume and intrinsic microporosity in polymers. *J. Mater. Chem.* **15**, 1977–1986 (2005)
- Calabro, V., Jiao, B., Drioli, E.: Theoretical and experimental study on membrane distillation in the concentration of orange juice. *Ind. Eng. Chem. Res.* **33**(7), 1803–1808 (1994)
- Clausing, P.: Über die stromung sehr verdünnter gas durch rohren von beliebiger lange. *Ann. Phys. (Leipzig)* **12**, 961–989 (1932)
- Clausing, P.: The flow of highly rarefied gases through tubes of arbitrary length. *J. Vac. Sci. Technol.* **8**(5), 636–756 (1971)
- Curcio, E., Drioli, E.: Membrane distillation and related operations—a review. *Sep. Purif. Rev.* **34**(1), 35–86 (2005)
- Davis, D.H.: Monte Carlo calculation of molecular flow rates through a cylindrical elbow and pipes of other shapes. *J. Appl. Phys.* **31**(7), 1169–1176 (1960)
- Diban, N., Voinea, O., Urriaga, A., Ortiz, I.: Vacuum membrane distillation of the main pear aroma compound: experimental study and mass transfer modeling. *J. Membr. Sci.* **326**(1), 64–75 (2009)
- Ermak, D.L., Mccammon, J.A.: Brownian dynamics with hydrodynamic interactions. *J. Chem. Phys.* **69**(4), 1352–1360 (1978)
- Evans, R. III., Watson, G., Mason, E.: Gaseous diffusion in porous media at uniform pressure. *J. Chem. Phys.* **35**(6), 2076–2083 (1961)
- Evans, R. III., Watson, G., Mason, E.: Gaseous diffusion in porous media. II. Effect of pressure gradients. *J. Chem. Phys.* **36**(7), 1894–1902 (1962)
- Flory, C.A., Cutler, L.S.: Integral equation solution of low-pressure transport of gases in capillary tubes. *J. Appl. Phys.* **73**(4), 1561–1569 (1993)
- Haddad, O.M., Abuzaid, M.M.: Effect of periodically oscillating driving force on basic microflows in porous media. *J. Porous Media* **9**(7), 695–707 (2006)
- Haddad, O.M., Abuzaid, M.M., Al-Nimr, M.A.: Developing free-convection gas flow in a vertical open-ended microchannel filled with porous media. *Numer. Heat Transf. A* **48**(7), 693–710 (2005)
- Haddad, O.M., Al-Nimr, M.A., Taamneh, Y.: Hydrodynamic and thermal behavior of gas flow in microchannels filled with porous media. *J. Porous Media* **9**(5), 403–414 (2006)
- Haddad, O.M., Al-Nimr, M., Al-Omary, J.: Forced convection of gaseous slip-flow in porous micro-channels under Local Thermal Non-Equilibrium conditions. *Transp. Porous Media* **67**(3), 453–471 (2007)
- Iczkowski, R.P., Iczkowski, R.P., Margrave, J.L., Margrave, J.L., Robinson, S.M., Robinson, S.M.: Effusion of gases through conical orifices. *J. Phys. Chem.* **67**(2), 229–233 (1963)
- Karniadakis, G., Beskok, A.: *Micro Flows—Fundamentals and Simulation*. Springer, New York (2002)
- Knudsen, M.: Die gesetze der molekularströmung und der inneren reibungsströmung der gas durch röhren. *Ann. Phys.* **333**(1), 75–130 (1909)
- Knudsen, M., Fisher, W.: The molecular and the frictional flow of gases in tubes. *Phys. Rev. (Ser. I)* **31**(5), 586–588 (1910)
- Kogan, A.: Direct solar thermal splitting of water and on-site separation of the products—ii. experimental feasibility study. *Int. J. Hydrogen Energy* **23**(2), 89–98 (1998)
- Krishna, R., Baten, J.M.van : A molecular dynamics investigation of the unusual concentration dependencies of Fick diffusivities in silica mesopores. *Micropor. Mesopor. Mater.* **138**(1-3), 228–234 (2011)
- Lawson, K.W., Lloyd, D.R.: Membrane distillation. II. Direct contact MD. *J. Membr. Sci.* **120**(1), 123–133 (1996)
- Lim, Y.I., Bhatia, S.: Simulation of methane permeability in carbon slit pores. *J. Membr. Sci.* **369**(1-2), 319–328 (2011)
- Mason, E., Malinauskas, A., Evans, R. III.: Flow and diffusion of gases in porous media. *J. Chem. Phys.* **46**(8), 3199–3216 (1967)
- Mulder, M.: *Basic Principles of Membrane Technology*. 2nd edn. Kluwer, Dordrecht (1996)
- Park, H.B., Jung, C.H., Lee, Y.M., Hill, A.J., Pas, S.J., Mudie, S.T., Wagner, E.V., Freeman, B.D., Cookson, D.J.: Polymers with cavities tuned for fast selective transport of small molecules and ions. *Science* **318**(5848), 254–258 (2007)
- Pollard, W.G., Present, R.D.: On gaseous self-diffusion in long capillary tubes. *Phys. Rev.* **73**(7), 762–774 (1948)
- Present, R.D., De Bethune, A.J.: Separation of a gas mixture flowing through a long tube at low pressure. *Phys. Rev.* **75**(7), 1050–1057 (1949)

- Qtaishat, M., Matsuura, T., Kruczek, B., Khayet, M.: Heat and mass transfer analysis in direct contact membrane distillation. *Desalination* **219**(1-3), 272–292 (2008)
- Reif, F.: *Fundamentals of Statistical and Thermal Physics*. McGraw-Hill, New York (1965)
- Reynolds, T.W., Richley, E.A.: Flux patterns resulting from free-molecule flow through converging and diverging slots. NASA Tech Note TN D-1864, pp 1–69 (1964)
- Reynolds, T.W., Richley, E.A.: Free molecule flow and surface diffusion through slots and tubes—a summary. NASA Technical Report TR R-255 (1967)
- Richley, E.A., Reynolds, T.W.: Numerical solutions of free-molecule flow in converging and diverging tubes and slots. NASA Tech Note TN D-2330, pp 1–45 (1964)
- Ruthven, D.M., Desisto, W.J., Higgins, S.: Diffusion in a mesoporous silica membrane: validity of the Knudsen diffusion model. *Chem. Eng. Sci.* **64**, 3201–3203 (2009)
- Steckelmacher, W.: Knudsen flow 75 years on: the current state of the art for flow of rarefied gases in tubes and systems. *Rep. Prog. Phys.* **49**, 1083–1107 (1986)
- Talley, W.K., Whitaker, S.: Monte Carlo analysis of Knudsen flow. *J. Comput. Phys.* **4**(3), 389–410 (1969)
- Villani, S.: *Isotope Separation*. American Nuclear Society, Hinsdale (1976)
- Walsh, J.W.T.: Radiation from a perfectly diffusing circular disc (part I). *Proc. Phys. Soc. Lond.* **32**, 59–71 (1919)
- Zhang, J., Gray, S., Li, J.D.: Modelling heat and mass transfers in DCMD using compressible membranes. *J. Membr. Sci.* **387**(388), 7–16 (2012)